Materials Advances

ROYAL SOCIETY OF CHEMISTRY

PAPER

View Article Online
View Journal

Check for updates

Cite this: DOI: 10.1039/d5ma01183c

Sulfation of thiol–maleimide crosslinked hydrogels modulates material properties and cell biocompatibility

Lasse Riediger,[a] Lei Wang,[ab] Peer Nölte,[c] Cosmin Butnarasu,[d] Peng Tang,[a] Yannic Kerkhoff,[ae] Elisa Quaas,[a] Justin Arenhoevel,[a] Daniel Lauster,[d] Yi-An Yang,*[a] Nan Ma*[a] and Rainer Haag †[a]

Sulfation has become a critical but still underexplored factor influencing hydrogel properties and regulating cell behaviour. In this study, a thiol–maleimide crosslinked hydrogel system based on a poly(*N*-isopropylacrylamide) (pNIPAM) copolymer and dendritic polyglycerol (dPG) was developed to systematically investigate how sulfation modulates material properties, material affinity and cell viability. Sulfated (dPGS) and non-sulfated dPG were crosslinked with pNIPAM copolymers *via* thiol–maleimide coupling to form hydrogels at temperatures suitable for cell cultivation. Sulfation increased the pore size (2.3-fold), enhanced gel strength (G' 466 *vs.* 334 Pa at 37 °C) and retarded enzymatic degradation, while maintaining similar thermoresponsive behaviour. FRAP revealed size-selective transport, with unchanged diffusion of small dextran (4 kDa) but a 21% reduction in albumin diffusion after sulfation, indicating efficient nutrient exchange while enabling partial retention of larger proteins. Biological evaluation demonstrated the enhanced cell viability of A549 and HeLa cells in the sulfated hydrogel, while MCF-7 cells showed a cell-type-specific response to sulfation. The dPGS-based hydrogel enhanced cell attachment and viability in a planar hydrogel substrate, and promoted spheroid formation and proliferation when cells were embedded within the 3D hydrogel network, mimicking a more physiologically relevant microenvironment. Overall, our findings identify sulfation as an effective handle to adjust thermoresponsive behaviour, macromolecular transport and cell-type-specific responses in thiol-crosslinked hydrogels, laying the basis for their use in advanced cell culture systems and, in the longer term, tissue-engineering-oriented applications.

Received 13th October 2025,
Accepted 28th December 2025

DOI: 10.1039/d5ma01183c

rsc.li/materials-advances

Open Access Article. Published on 30 December 2025. Downloaded on 2/25/2026 1:52:12 AM.
This article is licensed under a Creative Commons Attribution 3.0 Unported Licence.

Introduction

Hydrogel platforms have emerged as pivotal biomaterials in cell cultivation and tissue engineering applications, offering three-dimensional environments that closely mimic the native extracellular matrix. Recent advances in hydrogel engineering have demonstrated their potential to recapitulate complex tissue microenvironments and support diverse cellular functions.[1] In particular, synthetic hydrogels are attractive because their mechanical properties, degradation behaviour, and biochemical functionalities can be precisely tuned, which is highly relevant for applications in advanced *in vitro* cell culture and future regenerative medicine approaches.[1,2]

Thermoresponsive hydrogels provide unique advantages through their ability to undergo reversible phase transitions in response to physiological temperature changes, enabling controlled cell encapsulation, cultivation, and harvest without enzymatic treatment.[3–5] Despite significant advances in hydrogel design, current platforms often lack the precise control over mechanical properties, degradation kinetics, and biological functionality required for optimal cell cultivation across diverse cell types and applications. This challenge has driven the development of next-generation biomaterials with tuneable properties and enhanced bioactivity.[2] Recent work on multifunctional adhesive hydrogel patches and advanced wound dressings further illustrates how engineered hydrogel networks can integrate mechanical properties, bioactivity and stimulus-responsiveness for biomedical applications.[6]

[a] *Institute of Chemistry and Biochemistry, Freie Universität Berlin, Takustraße 3, 14195 Berlin, Germany. E-mail: yianyang@zedat.fu-berlin.de, nan.ma@fu-berlin.de, haag@zedat.fu-berlin.de*
[b] *Institute of Functional Materials for Sustainability Helmholtz-Zentrum Hereon, 14513 Teltow, Germany*
[c] *Institute of Macromolecular Research (BIMF) and Bavarian Polymer Institute (BPI), University of Bayreuth, Universitätsstr. 30, 95447 Bayreuth, Germany*
[d] *Institute of Pharmacy, Biopharmaceuticals, Freie Universität Berlin, 12169, Germany*
[e] *Zuse-Institut Berlin (ZIB), Takustraße 7, 14195 Berlin, Germany*
† Lead contact.

© 2026 The Author(s). Published by the Royal Society of Chemistry

Open Access Article. Published on 30 December 2025. Downloaded on 2/25/2026 1:52:12 AM.
This article is licensed under a Creative Commons Attribution 3.0 Unported Licence.

Thiol–maleimide crosslinking represents a highly efficient and bioorthogonal approach to hydrogel formation, utilizing the rapid and selective Michael addition reaction between thiol and maleimide functional groups. This crosslinking mechanism offers distinct advantages over other strategies, including rapid gelation kinetics under physiological conditions, excellent biocompatibility, and the absence of toxic byproducts or initiators.[7] Recent studies have further demonstrated the versatility of this chemistry, with applications ranging from injectable hydrogels for tissue repair to degradable networks for controlled drug release.[8] The thiol–maleimide reaction proceeds efficiently at neutral pH and physiological temperature, making it particularly suitable for cell encapsulation applications, where harsh crosslinking conditions must be avoided.[9] Moreover, the orthogonal nature of this chemistry allows for sequential functionalization and precise control over network architecture.[10]

In natural extracellular matrices (ECMs), sulfation is a critical modification that regulates cell behaviour and tissue function. For example, sulfated glycosaminoglycans (GAGs) such as heparan sulfate (HS) and chondroitin sulfate (CS) are integral components of the ECM, influencing major cellular processes, such as cell adhesion, migration, and differentiation by interacting with growth factors and cell surface receptors. Sulfated materials have also shown particular promise in mimicking the highly charged extracellular matrix and space found in cartilage and other connective tissues.[11,12] Following this natural paradigm, sulfated polysaccharides and synthetic sulfated polymers demonstrated enhanced protein binding capacity, cell adhesion, and modified diffusion characteristics compared to their non-sulfated counterparts.[13–15] Werner and Freudenberg have extensively investigated how sulfation patterns and charge density in GAG-based hydrogels influence cytokine sequestration and growth factor presentation, showing that controlled sulfation enables precise tuning of VEGF release and macrophage cytokine profiles.[16] Sulfate groups strongly affect electrostatic interactions within the hydrogel matrix, which in turn modulate both mechanical properties and biological performance by altering protein–material interactions and cellular signalling pathways.[17] Building on this concept, Zieris and Dockhorn *et al.* demonstrated that selective desulfation of heparin within starPEG–heparin hydrogels allows fine control of growth factor binding and release, effectively decoupling mechanical properties from biochemical functionality.[18] Similarly, Atallah *et al.* developed *in situ*-forming GAG hydrogels with varied sulfation patterns, enabling independent regulation of network mechanics, protein affinity, and stem cell behaviour, including sustained growth factor delivery and guided cell migration.[19,20] Collectively, these studies highlight that sulfation is not merely a structural feature but a versatile design parameter for modulating cell behaviour in both 2D and 3D matrices. However, these insights arise predominantly from naturally derived or GAG-based systems, while the impact of sulfation in purely synthetic, thermoresponsive hydrogel networks remains comparatively underexplored.

Poly(*N*-isopropylacrylamide) (pNIPAM)-based copolymer systems combined with dendritic polyglycerol (dPG) represent an innovative approach to thermoresponsive hydrogel design. pNIPAM exhibits a well-characterised lower critical solution temperature (LCST) of around 32 °C, enabling temperature-triggered phase transitions relevant to cell culture applications.[21,22] The precise tunability of the LCST through copolymerization has enabled the development of systems with transition temperatures optimized for specific biomedical applications.[23] The integration of dPG as a biocompatible, highly branched polyether provides enhanced water solubility, reduced cytotoxicity, and improved mechanical properties compared to linear polymer alternatives.[24,25] Dendritic architectures offer unique advantages in terms of multifunctionality and controlled presentation of bioactive groups.[25,26] In a modular pNIPAM–dPG scaffold, thermoresponsive behaviour is mainly governed by the pNIPAM backbone, while the charge density and protein affinity can be adjusted *via* sulfation of the dPG scaffold, providing a basis to disentangle these contributions in a fully synthetic hydrogel system.

Optimal diffusion behaviour within hydrogel networks is paramount for successful long-term cell cultivation, and efficient mass transport ensures adequate nutrient delivery, protein distribution, and cell transport throughout the entire gel matrix.[27,28] Mathematical modelling studies have established clear relationships between network structure, charge density, and diffusion coefficients for various molecular sizes.[29] Poor diffusion characteristics necessitate frequent cell harvesting, treatment with external factors, and re-encapsulation procedures that impose significant mechanical and chemical stress on cultured cells, potentially compromising cell viability and phenotype.[30] In contrast, hydrogel systems with optimized diffusion properties enable continuous, gentle cultivation protocols where cells and organoids can be maintained in their three-dimensional environment while allowing controlled delivery of growth factors, drugs, or other bioactive molecules without disrupting the culture system.[31] This approach is particularly advantageous for sensitive cell types and complex organoid cultures where mechanical manipulation should be minimized to preserve tissue architecture and cellular function.[32] The ability of sulfated hydrogels to modulate both diffusion and factor retention, as demonstrated in the above studies, highlights their potential to meet these stringent requirements for advanced organoid culture systems.[33] Such selective control over molecular transport and signalling is in line with broader efforts to use nanoscale structure and chemistry to regulate catalytic and biological responses, as exemplified by recent work on nanozyme systems with tunable selectivity.[34]

Comprehensive biological evaluation of hydrogel platforms requires assessment of cell viability across multiple cell lines to establish broad applicability and identify cell-type-specific responses. Fluorescence recovery after photobleaching (FRAP) measurements provide crucial insights into molecular diffusion processes within hydrogel networks, revealing how sulfation affects mass transport properties essential for nutrient delivery and waste removal in cell culture applications.[35]

© 2026 The Author(s). Published by the Royal Society of Chemistry

Open Access Article. Published on 30 December 2025. Downloaded on 2/25/2026 1:52:12 AM. This article is licensed under a Creative Commons Attribution 3.0 Unported Licence.

Advanced imaging techniques, including super-resolution microscopy and fluorescence correlation spectroscopy, have further enhanced our understanding of molecular transport in complex hydrogel networks.[36] Comparative analysis between sulfated and non-sulfated systems enables direct assessment of sulfation effects on both material properties and biological performance. The primary objective of this study was to systematically investigate the role of sulfation in thiol–maleimide crosslinked pNIPAM–dPG hydrogels for cell cultivation applications *in vitro*. We hypothesize that sulfation will significantly modulate hydrogel properties, including thermoresponsive behaviour, mechanical characteristics, and biological performance, providing design principles that may inform future development of synthetic hydrogels for tissue engineering and regenerative medicine.

Materials and methods

General information

Polyethylene glycol M_w 300 and *N*-isopropylacrylamide (NIPAM) were purchased from TCI (Zwijndrecht, Belgium). 2,2′-Azobis-(isobutyronitrile) (AIBN) was recrystallized from methanol before use. Dendritic polyglycerol amine (dPG-$NH_{2(8\%)}$) with an M_w of 7.4 kDa and a dispersity of 1.6 was kindly provided by Cathleen Schlesener and synthesized by a previously reported method of Hellmund *et al.* and characterised by ^{1}H-NMR and size exclusion chromatography (GPC).[37] Methansulfonyl chloride and sulfur trioxide pyridine complex were purchased from Sigma Aldrich (Darmstadt, Germany), *N*-succinimidyl 6-maleimidocaproate was acquired from abcr (Karlsruhe, Deutschland) and sodium azide was acquired from Fisher Scientific (Darmstadt, Germany).

Dialysis

All polymers were purified by dialysis using tubes with different molecular weight cut-offs (MWCO 1 kDa or 10 kDa) Spectra/Por™ 6 dialysis membranes purchased from Fisher Scientific (Darmstadt, Germany).

Nuclear magnetic resonance (NMR)

^{1}H NMR and ^{13}C NMR spectra were recorded either on a Bruker AVANCE III 500 (Bruker Corporation), or a Jeol ECZ600 (JEOL GmbH), or a Bruker AVANCE III 700 (Bruker Corporation). Chemical shifts are reported in δ (ppm) and referenced to the respective deuterated solvents.

Gel permeation chromatography (GPC)

GPC measurements were performed with a customized chromatography system and a differential refractometer was used to separate and analyse the samples. The mobile phase was DMF (10 mM LiBr) at a flow rate of 1.0 mL min^{-1}. The columns were heated at 50 °C, while the differential refractometer detector was kept at 35 °C. For each measurement, 50 µL of a prefiltered (PTFE 0.2 µm) 1.5 mg mL^{-1} sample solution was injected. The data were processed using the WinGPC unichrome software from PSS. Molecular weights and molecular weight distribution were obtained relative to a poly(methyl methacrylate) standard.

Infrared spectrometer

A Bruker Alpha II FT-IR spectrometer was used for the experiments.

Dynamic light scattering (DLS)

A Zetasizer Nano ZS (Malvern Instruments Ltd, Worcestershire, UK) equipped with a 4 mW HeNe laser (λ = 633 nm, NIBS) operating with a 173° scattering angle (backscatter). Particle size was measured in UV-transparent disposable cuvettes (UltraVette, 8.5 mm, Brand, Wertheim, Germany) at 25 °C. Samples were dissolved in PBS (10 mM, pH 7) at a concentration of 50 mg mL^{-1}. The solutions were filtered once through a 0.2 µm regenerated cellulose (RC) syringe filter (VWR International, Ismaningen, Germany). Samples were equilibrated for 60 s at 25 °C; subsequently, the measurement was performed with 15 scans per sample.

UV/Vis spectra

An Agilent Cary 8454 or Scinco S-3100 spectrometer using 1.5 mL polystyrene cuvettes was used.

Ellman's assay

The number of free, reactive thiol groups in pNIPAM-*co*-PEG-SH was determined using an Ellman's assay.[38] In this method, the model disulfide 5,5′-dithiobis-(2-nitrobenzoic acid) (DTNB) is quantitatively reduced by thiols, resulting in the release of the TNB^{2-} anion. The formation of TNB^{2-} was monitored by UV-vis spectroscopy, allowing for quantification of thiol groups per polymer relative to a calibration standard.

Hydrogel formation

Two working solutions (c = 100 mg mL^{-1}) of dPG(S)-$Mal_{(8\%)}$ and pNIPAM-*co*-PEG-$SH_{(10\%)}$ were prepared in 10 mM PBS. pNIPAM-*co*-PEG-$SH_{(10\%)}$-solution was diluted with 10 mM PBS to achieve the desired molar ratio of 1 : 1 (Mal : SH) and dPG(S)-$Mal_{(8\%)}$-solution with a concentration of 50 mg mL^{-1} was added. The gel was formed within 15 min and a biopsy punch was used to create 8 mm gel pellets.

Scanning electron microscopy (SEM)

All samples were lyophilized and sputtered with a thin layer of gold nanoparticles (~8–10 nm) under high vacuum using a sputter coater (Emscope SC 500, Quorum Technologies, UK). The surface morphology and hydrogel structures were investigated with a scanning electron microscope (Hitachi SU8030, Japan, at a high voltage of 10 kV, with a working distance of 8.3 mm). Hydrogel pellets with molar ratios of 1 : 1 (Mal : SH) of 50 mg mL^{-1} at 37 °C and 25 °C were investigated. The SEM images of hydrogels were analysed using a custom FIJI macro, with the minimal Feret diameter used as an indicator of pore size. Two image replicates per condition were analysed, and the resulting data were pooled.[39]

Open Access Article. Published on 30 December 2025. Downloaded on 2/25/2026 1:52:12 AM. This article is licensed under a Creative Commons Attribution 3.0 Unported Licence.

Rheology

The Malvern Instruments Kinexus was used for all measurements. Rheological tests on preformed gels were carried out using an 8 mm diameter plate that was adjusted in gap size to touch the gel. For the amplitude sweep, the measurement range was set as 0.1–5% at 1 Hz. For the frequency sweep, the range was set as 0.1–5 Hz at 1%, with a normal force of ~0.07 N. All rheological experiments were repeated in triplicates.

Fluorescence recovery after photobleaching (FRAP)

Fluorescence recovery after photobleaching (FRAP) experiments were conducted using a Leica TCS SP8 confocal laser scanning microscope (Leica Microsystems, Wetzlar, Germany) equipped with a 63× oil immersion objective. The 488 nm line of an argon laser was operated at 20% power. Hydrogel samples were prepared at 5 wt% concentration and loaded with either FITC-dextran (4 kDa) or FITC-labelled bovine serum albumin (FITC-BSA, Sigma Aldrich A9771) at a final tracer concentration of 2 μM (expressed as FITC). Samples were transferred to 15-well chambered glass coverslips (Ibidi μ-Slide, 170 ± 5 μm). A circular region of interest (ROI) with a radius of 3.6 μm was selected in the imaging field. Time-series acquisition consisting of five prebleach frames was acquired at 5% of the laser output (setting in LAS AF software), followed by bleaching at 100%. Fluorescence recovery was recorded for 67.8 s across three acquisition phases: an initial fast phase (0–7.6 s, 100 frames), a second phase (7.6–17.6 s, 10 frames), and a third phase (17.6–67.6 s, 10 frames). Fluorescence intensity within the ROI was normalized to the prebleach intensity. Recovery curves were fitted using an exponential fit model within the Leica LAS AF analysis tool to determine the characteristic diffusion time (τ). The apparent diffusion coefficient (D) was calculated using the equation: $D = \omega^2/(4\tau)$ where ω is the radius of the bleached region. All experiments were performed at room temperature. For each condition, measurements were performed in duplicate, with 10 independent replicates per sample.

Cell sources

A549, HeLa and MCF-7 cells were obtained from Leibniz-Institut DSMZ (Deutsche Sammlung von Mikroorganismen und Zellkulturen GmbH). HaCaT cells were purchased from American Type Culture Collection (ATCC, USA). Cells were cultured in Dulbecco's Modified Eagle Medium (DMEM) supplemented with 10% (v/v) FBS, 100 U mL^{-1} penicillin and 100 μg mL^{-1} streptomycin.

2D cell attachment assay with hydrogel

Hydrogel layers of dPG-gel and dPGS-gel were formed in a 96-well dish at 5 wt%. A549 and HaCaT cells were harvested and seeded in single cells on a 2D hydrogel surface at 5 × 10^4 cells per cm^2. Live/dead staining was performed with a live/dead™ viability/cytotoxicity kit (Thermo Fisher Scientific, Schwerte, Germany) and microscopy images were subsequently collected with a confocal microscope.

Hydrogel encapsulation protocol of A549 cells in 3D

A549 cells were dissociated into single cells, harvested with centrifugation, and resuspended in culture medium at 2 × 10^6 cells per mL. Both dPGS-mal, dPG-mal and Copol-SH solutions at 100 mg mL^{-1} were mixed with an equal volume of cell suspension to create a polymer/cell mixture for the final hydrogel formulation. To formulate the cell-laden hydrogel, either 10 μL of dPGS-mal/cell mixture or dPG-mal/cell mixture was mixed with 10 μL of Copol-SH/cell mixture and added to the bottom of the 24-well plates. The final mixture was incubated in room temperature for 15 minutes to yield a fully crosslinked hydrogel (5 wt%) with a final cell density of 1 × 10^6 cells per mL, and warm culture medium was subsequently added to enable the nutrients for the encapsulated cells. Live/dead staining of cells in the hydrogel was performed with a live/dead™ viability/cytotoxicity assay kit (Thermo Fisher L32250), and images of the staining results were taken with a confocal microscope and processed with ImageJ.

CCK8 assay

All cell experiments were conducted according to German genetic engineering laws and German biosafety guidelines in the laboratory (safety level 2). Cell viability was determined using a CCK-8 kit (Hycultec; Art. HY-K0301) according to the manufacturer's instructions.

For cytotoxicity evaluation with 2D cell culture, cells were seeded in a 96-well plate at a density of 5 × 10^4 cells per mL in 90 μL DMEM per well overnight at 37 °C and 5% CO_2. For cytotoxicity evaluation of polymers, 10 μL of sample (dissolved in PBS) were added in serial dilutions including dead (1% SDS) and living controls (Medium, PBS) and incubated for another 24 h at 37 °C and 5% CO_2.

For cytotoxicity evaluation of hydrogel, hydrogels were incubated with DMEM at 37 °C overnight at the same time. After 24 h incubation, the conditioned medium on top of the cells was discarded and replaced by medium on top of the solid hydrogels. For background subtraction, wells containing no cells but only reagent were used. After 24 h incubation medium was exchanged and 10 μL of CCK8 solution was added in each well. Absorbance (450 nm/650 nm) was measured after approximately 3 h incubation of the dye using a Tecan plate reader (SPARK, Tecan Group Ltd). Measurements were performed in triplicates and repeated three times. Cell viability was calculated by setting the non-treated control to 100% and the non-cell control to 0% after subtracting the background.

Cell-laden hydrogels underwent continuous cultivation in 24-well dishes, and a CCK-8 assay was performed at designated time points. A reagent–medium mixture containing 10% of CCK-8 reagent was added to each sample and incubated for 3 hours, then collected for absorbance measurement at 450 nm. Cell-free hydrogel samples were used as the background control for each group.

Statistical analysis

All experiments were performed at least in triplicate with $n \geq 3$ independent experiments. Data are presented as mean ± standard deviation. Mann–Whitney U tests were performed

© 2026 The Author(s). Published by the Royal Society of Chemistry

Open Access Article. Published on 30 December 2025. Downloaded on 2/25/2026 1:52:12 AM. This article is licensed under a Creative Commons Attribution 3.0 Unported Licence.

for the SEM data and to assess statistically significant differences in medians, with significance set at $p < 0.001$. An unpaired *t*-test was used for the data from the cell image analysis, dextran diffusion and FRAP experiment. For the CCK-8 data, one-way ANOVA was used to assess statistically significant differences.

Synthetic procedures

Synthesis of PEG–acrylate (PEGA). Acrylation of polyethylene glycol was accomplished in dry conditions under an argon environment. PEG300 (M_n = 300, 6.8 g, 22.7 mmol, 1.0 eq.) was dried overnight at 40 °C under high vacuum and dissolved in dry DCM (30 mL) in a Schlenk flask. Triethylamine (4.7 mL, 34.1 mmol, 1.5 eq.) was added, and the mixture was cooled to 0 °C. Acryloyl chloride (2.8 mL, 34.1 mmol, 1.5 eq.) was dissolved in dry DCM (10 mL) and added dropwise to the reaction mixture at a rate of 11 mL per hour. The reaction was allowed to reach room temperature and stirred overnight. Methanol was used to quench the reaction. Solvents were removed using a rotary evaporator, and the product was obtained as a colorless oil (25% yield) after purification with column chromatography and analysed using ^{1}H-NMR.

Synthesis of pNIPAM-*co*-PEG-OH (Copol-OH). Free radical polymerization was used to copolymerize *N*-isopropylacrylamide (NIPAM) and PEGA, slightly altering a previously described method.[40] NIPAM (2.9 g, 25.7 mmol, 1.0 eq.), PEGA (2.3 g, 6.4 mmol, 0.25 eq.), and azobisisobutyronitrile (AIBN) (0.08 g, 0.48 mmol, 1.5 mol%) were dissolved in dry THF (60 mL) in a flask. The mixture was flushed with argon for two hours. The reaction proceeded for 24 hours while stirring at 60 °C. The solution was cooled to room temperature and concentrated using a rotary evaporator. The crude product was purified by dialyzing against water (M_w cut-off 10 kDa), lyophilized, and analysed using ^{1}H-NMR, ^{13}C-NMR, and GPC.

Synthesis of Copol-Oms. Copol-$OH_{10\%}$ (M_n = 12.0 kDa, 3.5 g, 23.4 mmol, 1.0 eq.) was dissolved in dry DMF (60 mL). After adding triethylamine (1.5 mL, 10.5 mmol, 3.0 eq./OH), the mixture was cooled down to 0 °C. Separately, methanesulfonyl chloride (0.8 mL, 10.5 mmol, 3.0 eq./OH) was dissolved in dry DMF (20 mL) and added dropwise to the suspension. The ice bath was withdrawn after 30 minutes of stirring at 0 °C, and the reaction proceeded overnight at room temperature. The crude product was dialyzed against water (M_w cut-off 1 kDa), lyophilized, and analysed using ^{1}H-NMR and ^{13}C-NMR.

Synthesis of Copol-SH. Copol-$OMs_{10\%}$ (1.0 g, 6.89 mmol, 1.0 eq./OMs) and thiourea (0.262 g, 3.445 mmol, 5 eq./OMs) were added to DMF (50 mL). After 3 days, water (20 mL) and sodium carbonate (0.110 g, 1.034 mmol, 1.5 eq./OMs) were added to the reaction. The reaction was quenched with MeOH (20 mL). The initially formed disulfide-crosslinked hydrogel was cleaved by DTT (0.117 g, 0.758 mmol, 1.1 eq./OMs) and was dialyzed against water (pH = 6; M_w cut-off 1 kDa), lyophilized, and analysed using ^{1}H-NMR, ^{13}C-NMR and Ellman's assay.

Synthesis of dendritic polyglycerol-azide (dPG-N_3). dPG-OH (M_n = 4.4 kDa, 8.4 g, 1.1 mmol, 1.0 eq.) was dried overnight at 40 °C under reduced pressure and dissolved in dry DMF (70 mL). Triethylamine (1.5 mL, 10.8 mmol, 1.2 eq./OH) was added, and the mixture was cooled to 0 °C. Methanesulfonyl chloride (0.8 mL, 10.5 mmol, 1.2 eq./OH), dissolved in dry DMF (15 mL), was added dropwise to the suspension. After stirring at 0 °C for 30 minutes, the ice bath was removed, and the reaction proceeded overnight at room temperature to yield the mesylated intermediate. The solution was filtered, and NaN_3 (1.8 g, 26.9 mmol, 3.0 eq./OMs) was added to convert the mesylate groups into azide groups. The crude product was purified by dialysis against MeOH and water (M_w cut-off 1 kDa) and lyophilized to obtain dPG-N_3. It was analysed using ^{1}H-NMR, ^{13}C-NMR, IR and zeta-potential.

Synthesis of dPGS-N_3. dPG-$N_{3(8\%)}$ (3.3 g, 42.2 mmol, 1.0 eq.) was dried overnight at reduced pressure and dissolved in dry DMF (75 mL) under inert conditions. The SO_3·pyridine complex (10.0 g, 63.3 mmol, 1.5 eq./OH) was dissolved in dry DMF (50 mL) and added *via* a syringe pump over 1 hour. The mixture was heated to 65 °C and stirred overnight. The crude product was purified by dialysis against brine and water (M_w cut-off 1 kDa) and lyophilized to obtain sulfated dPGS-N_3. It was analysed using ^{1}H-NMR, ^{13}C-NMR, GPC, EA and zeta-potential. The degree of sulfation of dPGS was quantified by elemental analysis of the sulfur content and calculated according to eqn (S2) in the SI.

Synthesis of dPG(S)-NH_2. The azide groups of dPG-$N_{3(8\%)}$ or dPGS-N_3 (M_n = 4.4/9.3 kDa, 4.5 g, 0.5625 mmol, 1.0 eq.) were reduced to amine groups. The polymer was dissolved in THF (175 mL). Triphenylphosphine (3.8 g, 14.51 mmol, 3.0 eq./N_3) was added, and the mixture was stirred for one hour at room temperature. Water (35 mL) was added, and the reaction mixture was continuously stirred at room temperature for three days. The conversion was monitored by IR spectroscopy. The crude product was purified by dialysis against MeOH and water (M_w cut-off 1 kDa) and lyophilized to obtain dPG-NH_2 or dPGS-NH_2. Characterization was performed using NMR and IR spectroscopy.

Synthesis of dPG(S)-Mal. The amine groups of dPG-$NH_{2(8\%)}$ or dPGS-$NH_{2(8\%)}$ (1.5 g, 20.27 mmol, 1.0 eq.) were functionalised with maleimide groups. The polymer was dissolved in PB-buffer (10 mL, 10 mM, pH = 8.1) and DMF (5 mL). Mal-NHS (0.9 g, 3.1 mmol, 1.5 eq./NH_2-group) was added, and the solution was stirred overnight. The crude product was purified by dialysis against MeOH and water (M_w cut-off 1 kDa). Characterization was performed by ^{1}H-NMR and ^{13}C-NMR.

Results and discussion

The hydrogels were prepared through covalent crosslinking of maleimide functionalised dendritic polyglycerol (dPG) or its sulfated derivative (dPGS) with thiolated pNIPAM-*co*-PEG copolymer (Copol-SH) *via* thiol–maleimide click chemistry. First, all polymer components were functionalised accordingly. The synthesis of the Copol-SH was achieved *via* a multi-step reaction starting from a precursor polymer (a–c, Fig. 1). The dPG maleimide-functionalised polymer (dPG(S)-Mal) was synthesized through a sequence of reactions (step d, Fig. 1).

Open Access Article. Published on 30 December 2025. Downloaded on 2/25/2026 1:52:12 AM.
This article is licensed under a Creative Commons Attribution 3.0 Unported Licence.

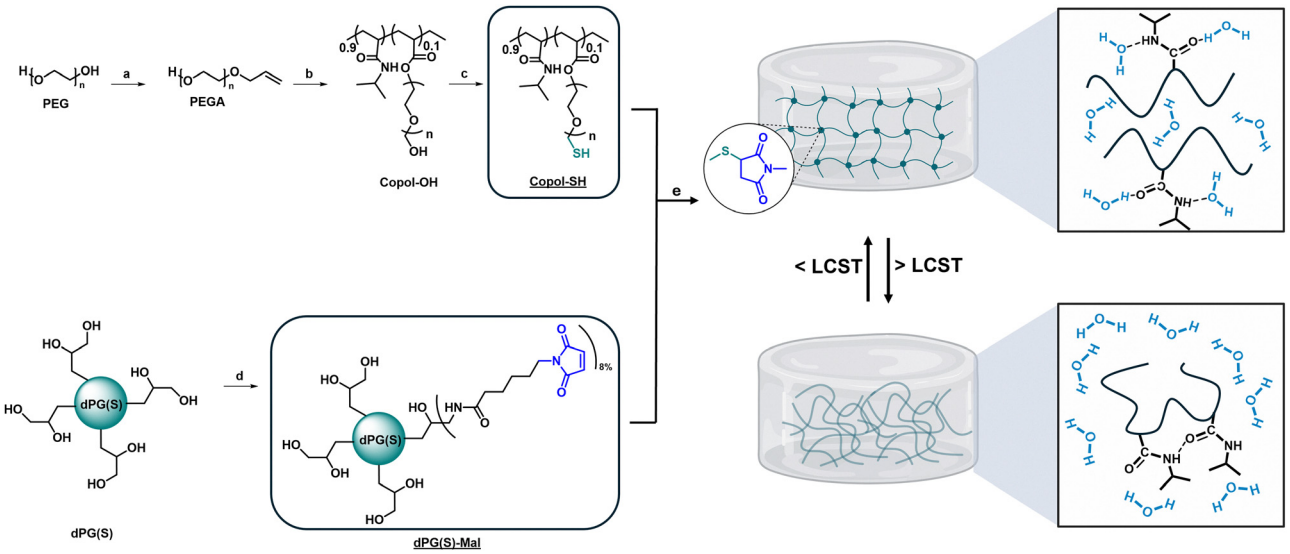

Fig. 1 Schematic illustration of hydrogel formation *via* thiol–maleimide click chemistry. The dendritic polyglycerol (dPG) or sulfated dendritic polyglycerol (dPGS) components are crosslinked by a molecule containing both thiol (–SH) and maleimide groups. This reaction forms a stable, covalently crosslinked network, resulting in the hydrogel structure shown on the right. The magnified view highlights the chemical linkage formed between a thiol group and a maleimide group within the hydrogel network. (a) Acryloylchloride, ET_3N, DCM, 0 °C-rt, 24 h; (b) NIPAM, AIBN, THF, 60 °C, 24 h; (c) 1. Mesylchloride, ET_3N, DMF, 0 °C-rt; 24 h; 2. Thiourea, Na_2CO_3 DMF/H_2O, rt, 72 h, 3. DTT, DMF/H_2O, 2 h; (d) 1 mesylchloride, ET_3N, DMF, 0 °C-rt, 24 h, 2. NaN_3 DMF, 60 °C, 72 h, 3. PPh_3, DMF/H_2O, rt, 72 h, 4. Mal-NHS, PB (10 mM, pH = 8.1), rt, 24 h; (e) hydrogel formation: Thiol : Mal molar ratio 1 : 1, 5 wt%, illustrating the thermoresponsive behaviour of the pNIPAM component at the LSCT. Created partial in BioRender.

The final hydrogel formation was initiated by the rapid and efficient reaction between the thiol groups of Copol-SH and the maleimide groups of dPG(S)-Mal in aqueous solution. The crosslinking reaction was performed at a thiol to maleimide molar ratio of 1 : 1 and a total polymer concentration of 5 wt% (e, Fig. 1). This approach yielded a stable, covalently crosslinked network. A schematic overview of the synthesis concept and the resulting network structure is shown in Fig. 1. The thiol–maleimide chemistry provides several advantages over other crosslinking strategies. This bioorthogonal reaction proceeds rapidly under physiological conditions without toxic initiators or harsh reaction conditions, making it ideal for cell encapsulation applications. Moreover, recent advances in thiol–maleimide chemistry have revealed thiol–maleimide bonds are susceptible to radical-mediated degradation, providing controllable degradation pathways for biomedical applications.[41] The 1 : 1 stoichiometric ratio ensures complete crosslinking while maintaining reproducible mechanical properties, as confirmed in our rheological analysis.

Surface topography of dPG and dPGS hydrogels

Scanning electron microscopy (SEM) was employed to visualize the internal morphology of the dPG- and dPGS-based hydrogels (A–D, Fig. 2). The analysis revealed that both hydrogel types exhibit a macroporous and homogeneous pore structure. At 25 °C, dPGS-based hydrogels displayed a significantly larger average pore diameter of 6.87 ± 5.61 μm compared to dPG-based hydrogels with 2.93 ± 2.96 μm, representing a 2.3-fold increase. This difference reflects the higher swelling capacity of the sulfated variant, attributable to the increased negative charge density.

Upon incubation above the lower critical solution temperature (LCST) at 37 °C, both hydrogel types showed a pronounced reduction in pore size. The pore diameter of the dPGS gels decreased by 54% to 3.14 ± 1.71 μm, while the pore diameter of the dPG gels decreased by 51% to 1.45 ± 1.38 μm. This observation is consistent with the thermoresponsive collapse of the pNIPAM network at elevated temperatures. The extent of the thermally induced structural transition was comparable for both hydrogel types (54% *vs.* 51% reduction). The relatively large standard deviations reflect the broad pore size distributions obtained from the SEM images. To ensure statistical reliability, pore diameters were quantified from multiple regions and a large number of pores per condition. The resulting datasets are visualised as a violin plot (Fig. S4), which clearly shows skewed, non-normal distributions and consistent shifts between the different conditions. These structural changes were also evident macroscopically. Photographic images (E–H, Fig. 2) demonstrated clear optical alterations in the appearance of the gels upon temperature increase, further confirming the thermoresponsive nature of the system. The significantly larger initial pore size of dPGS-based hydrogels can be attributed to the increased negative charge density from sulfation, which creates electrostatic repulsion between polymer chains and leads to enhanced swelling. This structural modification likely influences mass transport properties, as larger pores are expected to facilitate more efficient diffusion of nutrients and proteins. The comparable thermoresponsive collapse (54% in dPGS *vs.* 51% in dPG pore size reduction from 25 °C to 37 °C) indicates that sulfation does not compromise the fundamental pNIPAM switching mechanism, preserving

© 2026 The Author(s). Published by the Royal Society of Chemistry

Open Access Article. Published on 30 December 2025. Downloaded on 2/25/2026 1:52:12 AM.
This article is licensed under a Creative Commons Attribution 3.0 Unported Licence.

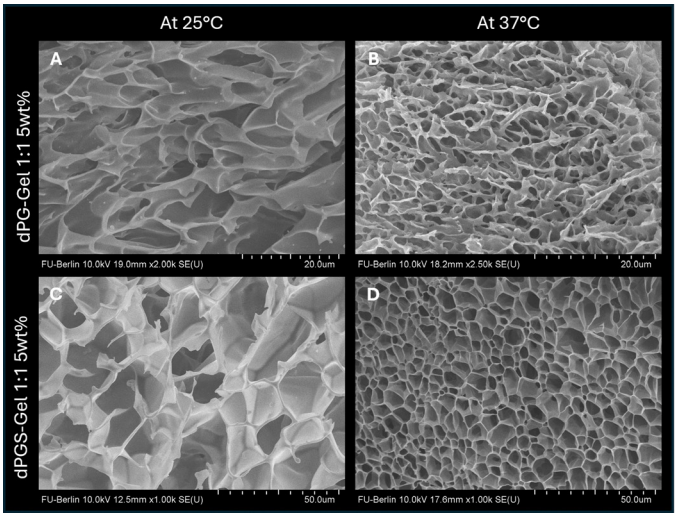

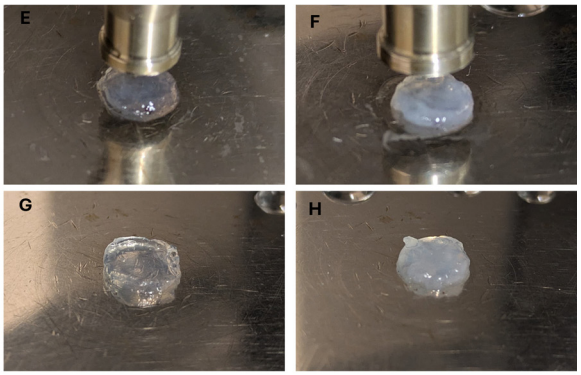

	25°C	37°C
dPG-Mal - Gel	2.93 ± 2.96 μm	1.45 ± 1.38 μm
dPG**S**-Mal - Gel	6.87 ± 5.61 μm	3.14 ± 1.71 μm

Fig. 2 SEM images of dPG-based (A 25 °C, B 37 °C) and dPGS-based (C 25 °C, D 37 °C) hydrogels at 25 °C, showing homogeneous macroporous network structures. Photographs (E)–(H) illustrate the temperature-dependent changes in gel appearance. Quantitative pore size analysis is summarized in the table. Data are shown as mean ± SD.

the temperature-triggered functionality essential for controlled cell cultivation applications. The high variability observed in pore sizes, particularly for dPGS hydrogels, reflects the heterogeneous nature of the crosslinked network structure. This finding aligns with work by Thönes *et al.* (2016),[42] who demonstrated that dPGS-based systems can effectively mimic the polyanionic extracellular matrix environment while maintaining responsive behaviour.[11]

Thermoresponsive rheological behavior

The viscoelastic properties of dPG and dPGS hydrogels were assessed by dynamic rheology at 25 °C and 37 °C across a frequency range of 0.1 to 1.0 Hz (A, B, Fig. 3). At 25 °C, dPG exhibited a storage modulus (G') of approximately 379 Pa at 1 Hz, which was significantly higher than its loss modulus (G'') of approximately 5.5 Pa, indicating a predominantly elastic, gel-like structure with high stiffness. dPGS at 25 °C also displayed a storage modulus (G') of approximately 334 Pa at 1 Hz, consistently higher than its loss modulus (G'') of approximately 1.1 Pa. G' for dPGS increased with frequency, showing a more pronounced frequency dependence compared to dPG. Overall, the rheological profiles of dPG and dPGS at 25 °C were qualitatively similar, with dPGS showing slightly lower absolute G' values and a stronger frequency dependence of G'.

Upon increasing the temperature from 25 °C to 37 °C, a significant increase in the shear moduli was observed for both hydrogels at 1 Hz. At 37 °C, the G' for dPG increased to approximately 400 Pa, while its G'' increased to approximately 28.6 Pa. For dPGS, the G' at 37 °C rose markedly to approximately 466 Pa, with G'' increasing to approximately 24.2 Pa. This pronounced increase in stiffness at 37 °C compared to 25 °C clearly demonstrates the thermoswitch behaviour mediated by the pNIPAM component, where the gel stiffens above the LCST. At 37 °C, both dPG and dPGS maintained their gel-like state with G' consistently and significantly higher than G'' across the frequency range. In contrast to the trend observed at 25 °C, dPGS exhibited higher modulus values than dPG at 1 Hz at 37 °C. This reversal in relative stiffness may be attributed to the influence of sulfation on the hydrogel's water content and network structure at elevated temperatures. Fig. 1 provides a schematic representation illustrating the network structure and hydrogen bonding interactions contributing to this thermoresponsive behaviour.

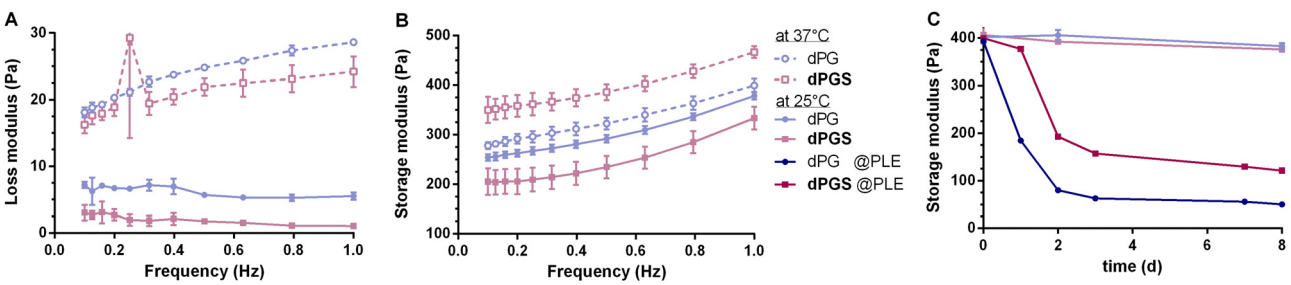

Fig. 3 Rheological properties of dPG and dPGS hydrogels at 25 °C and 37 °C. Loss modulus (A) (G'') and storage modulus (B) (G') are shown as a function of frequency. (C) Degradation behaviour of dPG and dPGS hydrogels over 8 days in the presence of porcine liver esterase (PLE) and control conditions.

Open Access Article. Published on 30 December 2025. Downloaded on 2/25/2026 1:52:12 AM.
This article is licensed under a Creative Commons Attribution 3.0 Unported Licence.

Consistent with the temperature-dependent mechanical response, the swelling behaviour of the hydrogels revealed a pronounced contraction when the temperature was increased from 25 °C to 37 °C (Fig. S5). At 25 °C, dPGS hydrogels exhibited a swelling ratio of 112.4 ± 2.0% and dPG hydrogels 114.4 ± 11.7%. Upon heating to 37 °C, a significant decrease in swelling was observed for both systems, with dPGS gels contracting to 75.6 ± 4.6% and dPG gels to 92.8 ± 2.9%. In those repeated temperature cycling both dPG and dPGS-gels remained essentially constant over several cycles, indicating reversible thermoresponsive volume changes without a systematic loss of swelling capacity in the investigated time frame. This deswelling effect was more pronounced for dPGS, reflecting a stronger thermoresponsive collapse of the sulfated network. The enhanced sensitivity of dPGS hydrogels is likely driven by sulfation-induced changes in hydrogen bonding and the hydration shell of the polymer chains, which reduce water retention at elevated temperatures. These findings corroborate the rheological data and highlight the critical role of sulfation in governing the thermal responsiveness of the hydrogel network.

The degradation kinetics of dPG and dPGS were evaluated by monitoring the change in shear modulus over 8 days in the presence of porcine liver esterase (PLE) or control buffer (C, Fig. 3). Under control conditions, both dPG and dPGS hydrogels maintained stable shear moduli near their initial values (approximately 400 Pa) over the 8-day period, indicating stability in the absence of the enzymatic stimulus. In the presence of PLE, both hydrogels underwent degradation, evidenced by a decrease in shear modulus. The dPG hydrogel exhibited rapid degradation, with its shear modulus dropping sharply within the first day and reaching values below 100 Pa by day 2. Degradation continued at a slower rate thereafter. The dPGS hydrogel also degraded in the presence of PLE, but at a significantly slower rate compared to dPG. The shear modulus of dPGS decreased more gradually, remaining above 200 Pa at day 2 and above 100 Pa at day 8. This indicates that the sulfation of dPGS confers increased resistance to PLE-mediated degradation. The rheological data reveal several key insights into the structure–property relationships of these hydrogel systems. The slightly lower initial modulus of dPGS at 25 °C (334 *vs.* 379 Pa) can be attributed to the increased swelling and larger pore sizes observed in SEM analysis. However, the reversal at 37 °C, where dPGS exhibits higher modulus values (466 *vs.* 400 Pa), suggests complex interactions between sulfation, hydration, and network structure at elevated temperatures. The enhanced resistance to enzymatic degradation in dPGS hydrogels likely results from the polyanionic nature of the sulfated network, which may sterically hinder enzyme access to cleavable bonds or alter the local microenvironment around susceptible sites. This tuneable degradation behaviour is particularly valuable for applications requiring controlled material resorption rates, such as tissue engineering scaffolds or drug delivery systems.[43]

Diffusion properties

To characterize the diffusion behaviour of macromolecules within dendritic polyglycerol (dPG) and sulfated dendritic polyglycerol (dPGS) hydrogels, fluorescence recovery after photobleaching (FRAP) experiments were conducted using FITC-labelled dextran (4 kDa) and FITC-labelled bovine serum albumin (BSA-FITC) as model solutes. The fluorescence recovery curves for FITC–dextran revealed rapid and nearly complete recovery in both hydrogel types (Fig. 4), indicating high diffusivity and minimal steric hindrance. The mobile fraction reached 95.2 ± 2.3% in dPG and 91.5 ± 3.1% in dPGS gels, while the corresponding diffusion coefficients were 0.244 ± 0.037 $\mu m^2\ s^{-1}$ and 0.246 ± 0.078 $\mu m^2\ s^{-1}$, respectively. These results suggest that the small, neutral dextran molecules are able to diffuse freely within both hydrogel matrices, with no significant difference between the two systems ($p > 0.05$), indicating that sulfation does not impair the transport of small molecules essential for cellular metabolism.

In contrast, FITC–albumin displayed lower diffusion than FITC–dextran in both matrices, with substantially reduced

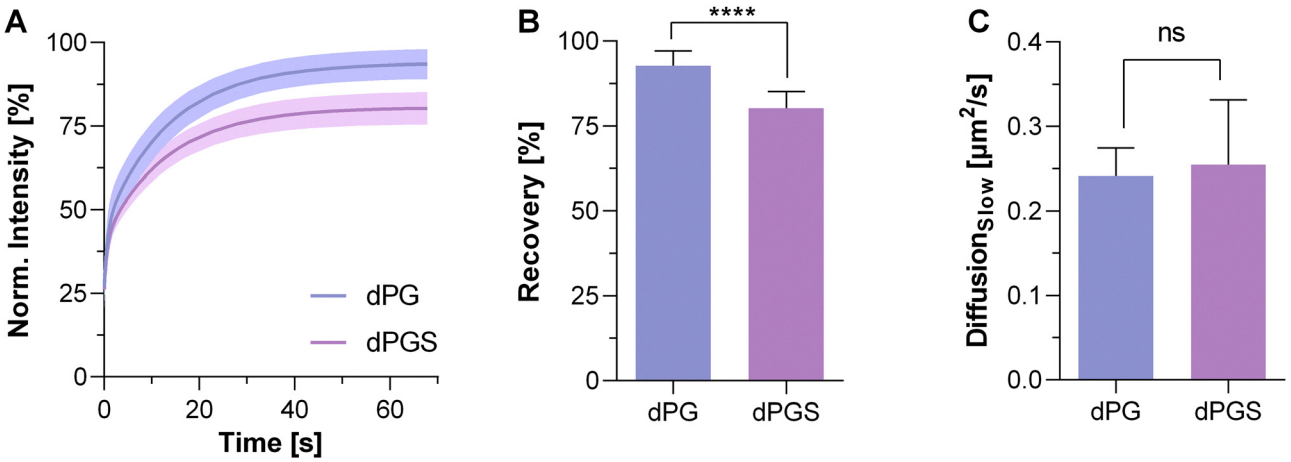

Fig. 4 FRAP analysis of FITC–dextran (4 kDa) diffusion in dPG and dPGS hydrogels. (A) Normalized fluorescence recovery over time. (B) Quantified mobile fraction of FITC–dextran. (C) Diffusion kinetics. Both hydrogels show high diffusivity, with slightly slower recovery and lower mobility in dPGS. Data shown as mean ± SD. Ns, not significant, ****, $p < 0.0001$.

© 2026 The Author(s). Published by the Royal Society of Chemistry

Open Access Article. Published on 30 December 2025. Downloaded on 2/25/2026 1:52:12 AM. This article is licensed under a Creative Commons Attribution 3.0 Unported Licence.

fluorescence recovery (Fig. S6B). The mobile fraction in dPG hydrogels was 55.2 ± 18.3%, compared to only 45.4 ± 14.9% in dPGS hydrogels. The diffusion coefficients for albumin were 0.263 ± 0.134 $\mu m^2\ s^{-1}$ in dPG and 0.208 ± 0.078 $\mu m^2\ s^{-1}$ in dPGS hydrogels, representing a 21% reduction in diffusivity within the sulfated system (Fig. S6C). The restricted mobility is attributed to both size exclusion effects and specific interactions between albumin and the hydrogel network. The further reduction in diffusion within dPGS hydrogels suggests additional electrostatic interactions between the negatively charged sulfate groups and positively charged regions on the albumin surface. Similar interactions have been described for other sulfated polymers such as heparin, known to form non-covalent, multivalent complexes with serum proteins including albumin.[44,45] The combination of steric hindrance and reversible binding likely contributes to the observed decreased mobile fraction and reduced diffusion coefficient.

Overall, the results demonstrate that hydrogel composition, particularly the presence of sulfate functionalities, significantly affects the diffusion of macromolecular solutes. While small neutral molecules like dextran show comparable diffusion coefficients in both systems (0.244 *vs.* 0.246 $\mu m^2\ s^{-1}$), larger proteins such as albumin show markedly reduced mobility in dPGS hydrogels (0.263 *vs.* 0.208 $\mu m^2\ s^{-1}$, 21% reduction). These findings are relevant for the design of hydrogel-based biomaterials where controlled diffusion, retention, or protein interaction is desired. The strong anionic charge of dPGS networks is expected to promote electrostatic association and prolonged residence of cationic cargos. Similar interactions have been used in dPGS nanocarriers to load and retain cytostatic drugs such as doxorubicin or paclitaxel.[46,47] In our hydrogels, this concept is mirrored by reduced albumin mobility while small, neutral solutes still diffuse efficiently.

The cell viability of the individual polymer components was quantitatively assessed using A549, HeLa, and MCF-7 cell lines (A, Fig. 5). Both dPGS-Mal and dPG-Mal (1 mg mL^{-1}) exhibited high cell viability in A549 and HeLa cells (>90%), comparable to the PBS control. In MCF-7 cells, dPGS-Mal showed moderately reduced viability (76.9 ± 1.8%), whereas dPG-Mal maintained high compatibility (96.5 ± 6%). Copol-SH induced a marked reduction in viability in HeLa (45% ± 8%) and MCF-7 (63% ± 4%) cells, while A549 cells remained unaffected (108% ± 5%). SDS, as the positive control, resulted in complete loss of viability. The reduced CCK-8 readout for HeLa and MCF-7 in the presence of Copol-SH indicates that this thiolated pNIPAM precursor is not equally well tolerated by all cell lines. HeLa and MCF-7 are more sensitive than A549, which remains close to the control. This is likely due to the reactive thiol groups, used at comparatively high local concentrations during hydrogel formation.

Hydrogels formed from dPGS and dPG (5 wt%) were evaluated for their effect on cell viability (B, Fig. 5). For A549 cells, both hydrogels supported high viabilities. In HeLa cells, a moderate decrease was observed for dPGS-gel (76% ± 4%), with a more pronounced reduction for dPG-gel (60% ± 5%). Notably, MCF-7 cells displayed the lowest viability within dPGS-gel (53% ± 4%), while dPG-gel maintained high compatibility (96% ± 7%). PBS controls confirmed high viability; SDS led to complete cytotoxicity. The cell viability data reveal distinct, cell line-dependent effects of both polymer composition and hydrogel formulation. dPGS-Mal and dPG-Mal polymers demonstrated excellent cytocompatibility with A549 and HeLa cells, closely matching the PBS control. In contrast, MCF-7 cells exhibited moderately reduced viability in the presence of dPGS-Mal, suggesting a specific sensitivity of this cell line to the sulfated dendritic polyglycerol structure. Copol-SH induced significant cytotoxicity in HeLa and MCF-7 cells, highlighting the importance of polymer selection for different cellular contexts. Upon crosslinking into hydrogels, dPGS-gel maintained high viability for A549 cells but with a decrease for MCF-7 cells (53 ± 4%), whereas dPG-gel supported robust proliferation of MCF-7 (96 ± 7%). This pronounced difference underscores a potential negative effect of sulfation on MCF-7 cell survival within the hydrogel matrix, which was not observed for A549 or HeLa. The results indicate that sulfation can modulate cell–matrix interactions in a cell type-specific manner. Taken together with the polymer data, these findings suggest that the observed viability patterns arise from a combination of cell line-specific sensitivity to the thiolated pNIPAM precursor and composition dependent cell–material interactions in the crosslinked networks, rather than from a single toxic component alone.

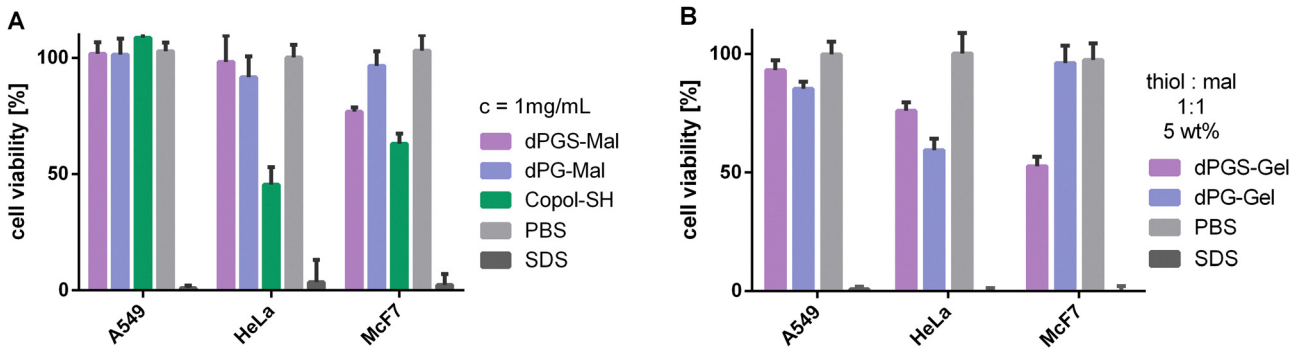

Fig. 5 (A) Cell viability of A549, HeLa, and MCF-7 cell lines after 24 h of exposure to different polymer components at 1 mg mL^{-1} and (B) hydrogels. Values are given as mean ± SD (n = 3). Data highlight the cell line-dependent effects of polymer composition and hydrogel formulation on cell viability.

Open Access Article. Published on 30 December 2025. Downloaded on 2/25/2026 1:52:12 AM.
This article is licensed under a Creative Commons Attribution 3.0 Unported Licence.

The cell-type-specific effects observed in this study may, among other factors, be influenced by differential accessibility of heparin-binding growth factors. Increased sulfation in hydrogels has been reported to enhance sequestration of such factors (*e.g.* FGF, VEGF) and to modulate their release kinetics and availability to cells.[48] These growth factors are strongly positively charged at physiological pH and are known to interact with sulfated glycosaminoglycans in the extracellular matrix. In our system, we did not directly quantify growth factor binding, but the reduced albumin mobility observed in FRAP, together with the stronger retention of cationic dyes in dPGS-gels compared to dPG-gels (alcian blue/methylene blue staining, Fig. S7), supports a higher affinity of the sulfated networks for positively charged biomolecules, in line with previous reports on heparin-mimetic sulfated polymers and dPGS.[14]

MCF-7 cells are well known as hormone- and growth factor-responsive breast cancer cells whose proliferation is controlled by oestrogens and mitogenic factors such as EGF and IGF signalling.[49] It is therefore plausible that changes in the effective availability of heparin-binding growth factors in a highly sulfated microenvironment have a stronger impact on MCF-7 than on the more robust carcinoma cell lines A549 and HeLa, which are typically maintained in standard serum-containing media without additional growth factor supplementation. Similar cell-type-specific effects arising from differences in growth factor dependence and receptor expression have been reported for sulfated and heparin-mimetic matrices, where the interplay between matrix-bound factors and cell surface receptors critically shapes cellular responses.[50] Reduced effective availability of such factors in highly sulfated environments could therefore contribute to the lower viability observed for MCF-7 cells in dPGS-Mal and dPGS-gels in our experiments. We emphasise that this mechanism remains a working hypothesis based on indirect evidence and literature comparison. Future studies will need to directly quantify growth factor binding. Taken together, our data indicate that the sulfation state of the hydrogel is a relevant parameter that must be carefully tailored to the requirements of specific cell types and applications.

The reduced viability of MCF-7 cells with dPGS-Mal and dPGS-gel suggests that this breast cancer cell line may be particularly sensitive to highly sulfated environments, possibly due to differences in membrane composition or cellular response pathways.[51,52]

This finding warrants further investigation into the underlying mechanisms, as it could provide insights into selective targeting strategies for cancer therapy applications. Future work should focus on optimising sulfation degrees to balance enhanced transport properties with broad cell-type compatibility. Spheroid formation within hydrogels is a key indicator for assessing hydrogel porosity as well as cell compatibility.

We further examined how sulfation of the hydrogel influences cell–material affinity and cell survival in both 2D and 3D

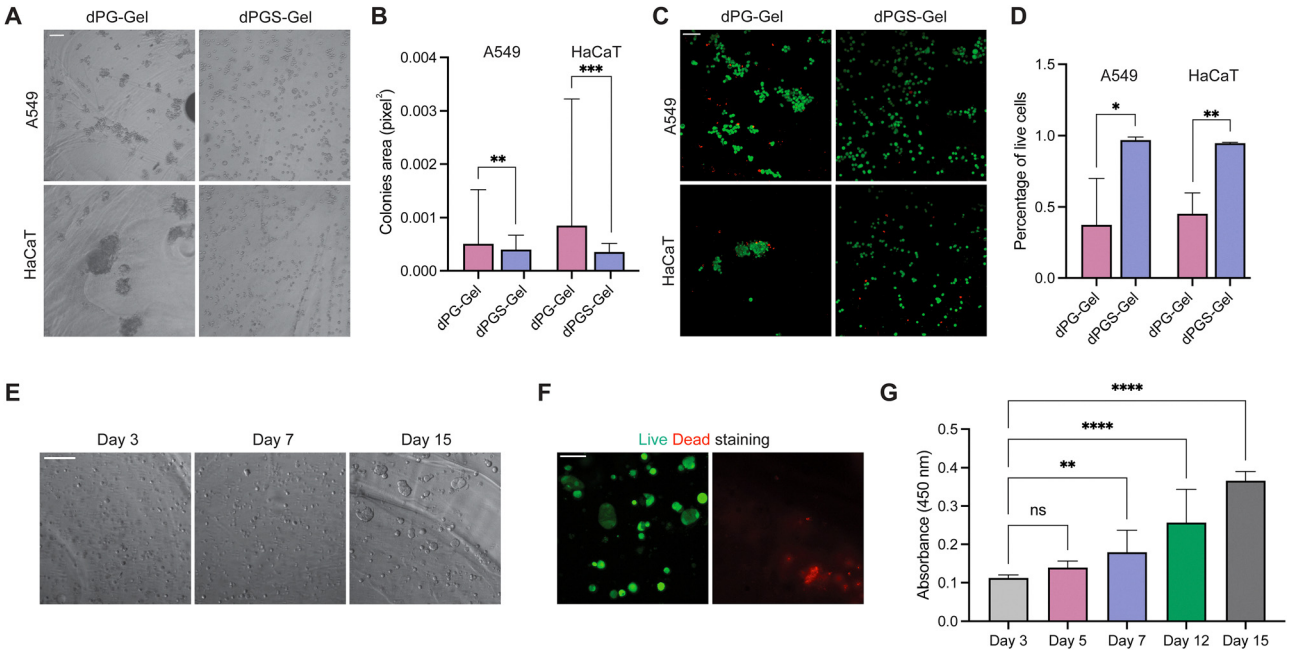

Fig. 6 Sulfated hydrogel supports cell growth in 2D and 3D cultivation. (A) Brightfield microscopy image of 2D cultivation of A549 cells and HaCaT cells on the 2D surface of dPG-gel and dPGS-gel on Day 1, scale bar 100 μm. (B) Live/dead staining of A549 cells and HaCaT cells in dPG-gel and dPGS-gel after 25 h, scale bar 100 μm. (C) Percentage of live A549 and HaCaT cells on the 2D surface of dPG-gel and dPGS-gel after 24 h (n = 3). (D) Colonies of area of live A549 and HaCaT cells on the 2D surface of dPG-gel and dPGS-gel after 24 h (n = 3). (E) Brightfield microscopy image of 3D cultivation of A549 cells in dPGS-gel on Day 3, 7 and 15 of continuous cultivation, scale bar 200 μm. (F) Live/dead staining of A549 cell spheroids in dPGS-gel on Day 13, scale bar 100 μm. (G) CCK-8 assay of A549 cell viability in dPGS-gel on Day 3, 5, 7, 12 and 15 (n = 3). Data are shown as mean ± SD. Ns, not significant, *, $p < 0.05$, **, $p < 0.01$, ***, $p < 0.001$, ****, $p < 0.0001$.

© 2026 The Author(s). Published by the Royal Society of Chemistry

Open Access Article. Published on 30 December 2025. Downloaded on 2/25/2026 1:52:12 AM. This article is licensed under a Creative Commons Attribution 3.0 Unported Licence.

culture. We decided to use tumour line A549, which was validated to grow normally under the existence polymers, and the non-tumour keratinocyte cell line HaCaT for testing. Cells were first seeded on the surface of 2D dPG- and dPGS-gel layers at 5 wt%. After 24 hours of seeding, the cells were more scattered in single cells and small clusters on the dPGS-gel surface as a result of cell–material attachment, compared with those on the dPG-gel surface that aggregated and formed more compact colonies (A and B, Fig. 6) that indicates enhanced cell–cell adhesion formation, which suggested the lower cell–material affinity of dPG-Gel. Both A549 and HaCaT cells also showed significantly higher viability on the 2D dPGS-gel compared with those on the dPG-gel (C and D, Fig. 6). These results indicate that sulfation of the hydrogel enhanced cell–material attachment and cell survival in 2D culture compared with the non-sulfated counterpart, which are in line with previous reports on sulfated matrices, where increased negative charge density has been shown to alter protein adsorption patterns and thereby regulate subsequent cell adhesion and behaviour.

We further evaluated the suitability of the dPGS-gel as a 3D scaffold for cell proliferation. A549 cells were chosen for the 3D encapsulation assay due to their high viability in reported polymers. In 3D culture, A549 cells encapsulated in dPGS-gels (5 wt%) formed compact spheroids that increased in size and metabolic activity over 15 days, indicating that the sulfated thermoresponsive network can sustain long-term cell growth (E and G, Fig. 6) and exhibited steady cell proliferation that was examined *via* CCK-8 assay (G, Fig. 6) during the 15-day continuous cultivation in dPGS-gel. These results demonstrate that the dPGS-gel is a structurally stable and highly biocompatible 3D scaffold that supports long-term cell cultivation, consistent with enhanced cell adhesiveness and survival observed in 2D culture.

Conclusions

The structural analysis by SEM revealed that both dPG- and dPGS-based hydrogels form macroporous networks. A key finding was the significantly larger initial pore size of dPGS-based hydrogels at 25 °C (5.2 μm) compared to dPG-based hydrogels (1.8 μm), directly correlating with the enhanced swelling capacity conferred by the increased negative charge density due to sulfation. Upon increasing the temperature to 37 °C, both hydrogel types exhibited a comparable and pronounced reduction in pore size (dPGS-gel: 46% decrease to 2.8 μm; dPG-gel: 44% decrease to 1.0 μm), confirming the robust thermoresponsive collapse of the pNIPAM network above its LCST. Macroscopic observations further corroborated this thermoresponsive behaviour.

Rheological characterization demonstrated that both hydrogels maintain a predominantly elastic, gel-like structure ($G' > G''$) across the tested frequency range at both 25 °C and 37 °C. At 25 °C, dPGS hydrogels showed slightly lower absolute modulus values and a more pronounced frequency dependence of G' compared to dPG. Notably, increasing the temperature to 37 °C resulted in a significant increase in shear moduli for both hydrogels, clearly illustrating the thermoswitch effect. At 37 °C, dPGS hydrogels exhibited higher modulus values than dPG, a reversal of the trend observed at 25 °C, which may be attributed to the complex interplay of sulfation-induced water content and network structure at elevated temperatures.

The degradation studies using porcine liver esterase (PLE) revealed that both hydrogels are susceptible to enzymatic degradation, evidenced by a decrease in shear modulus over time. Crucially, dPGS hydrogels demonstrated a significantly slower degradation rate compared to dPG hydrogels in the presence of PLE. This indicates that sulfation enhances the resistance of the hydrogel network to enzymatic cleavage, offering a mechanism to tune the degradation kinetics.

FRAP analysis provided crucial insights into the molecular transport properties of these hydrogel systems, revealing size-dependent diffusion behaviour that directly impacts their suitability for cell cultivation applications. Small molecules such as FITC–dextran (4 kDa) exhibited comparable diffusion coefficients in both systems (0.244 ± 0.037 μm^2 s^{-1} in dPG *vs.* 0.246 ± 0.078 μm^2 s^{-1} in dPGS) with mobile fractions of $95.2 \pm 2.3\%$ and $91.5 \pm 3.1\%$, respectively. This demonstrates that essential nutrients and metabolites can diffuse efficiently through both networks. In contrast, larger proteins like FITC–albumin (66 kDa) showed reduced diffusivity in dPGS hydrogels (0.208 ± 0.078 μm^2 s^{-1} *vs.* 0.263 ± 0.134 μm^2 s^{-1} in dPG, 21% reduction) with correspondingly lower mobile fractions ($59.8 \pm 3.7\%$ *vs.* $72.4 \pm 4.1\%$). This size-selective behaviour, attributed to electrostatic interactions between sulfate groups and proteins, suggests opportunities for controlled proliferation factor retention of larger biomolecules while maintaining adequate transport of small molecules essential for cellular metabolism. From a biological perspective, this indicates that diffusion of small nutrients and metabolites should remain efficient in both network types, whereas the mobility of larger serum proteins and signalling molecules is more strongly affected by sulfation. The combination of stable hydrogel mechanics, macroporous structure, and sustained viability suggests that mass transport of small nutrients and metabolites is not impaired, which is consistent with the high diffusion coefficients determined for 4 kDa dextran in both dPG and dPGS hydrogels. At the same time, FRAP experiments with FITC–albumin revealed a reduced mobile fraction and a 21% lower diffusion coefficient in dPGS-gels compared to dPG-gels, pointing to stronger, reversible interactions between proteins and the sulfated network. Although we did not directly quantify growth factor binding in this study, it is reasonable to assume that similar electrostatic interactions contribute to the local retention of positively charged, heparin-binding factors secreted by the cells. Such a mechanism would be in line with previous reports on sulfated and heparin-mimetic hydrogels, where charge-based sequestration and presentation of growth factors were shown to promote the formation and maintenance of cell aggregates. In our system, the concurrent observation of efficient small-molecule transport and slowed protein mobility therefore supports the notion that dPGS-based hydrogels

Open Access Article. Published on 30 December 2025. Downloaded on 2/25/2026 1:52:12 AM. This article is licensed under a Creative Commons Attribution 3.0 Unported Licence.

provide a microenvironment that combines nutrient supply with partial retention of larger biomolecules, which may facilitate spheroid formation and long-term proliferation. This interpretation, however, remains a hypothesis and will be addressed more directly in future work by dedicated growth factor binding and release studies. The continuous increase in CCK-8 signal over 15 days indicates that, under these conditions, mass transport and nutrient supply in dPGS-gels are sufficient to sustain long-term spheroid growth.

Cell viability assays with A549, HeLa, and MCF-7 cell lines highlighted the cell type-dependent cytocompatibility of the polymer components and the crosslinked hydrogels. While the individual dPG-Mal and dPGS-Mal polymers showed high viability for A549 and HeLa cells, MCF-7 cells exhibited reduced viability with dPGS-Mal. Upon crosslinking, dPGS-gel maintained high viability for A549 cells but resulted in a marked decrease for MCF-7 cells, whereas dPG-gel supported robust proliferation of MCF-7 cells. Proliferation assay on the 2D surface highlighted the enhanced cell–matrix affinity and cell survival rate provided by hydrogel sulfation, and 3D cell spheroid proliferation assay further evidenced the stability and biocompatibility of the sulfated hydrogel as a scaffold for 3D cell cultivation. These findings underscore that sulfation can modulate cell–matrix affinity and cell survival in a cell type-specific manner, necessitating careful consideration of hydrogel chemistry for specific cellular applications. As the present biocompatibility assessment was performed with tumour cell lines as well as keratinocytes, further studies are required to optimize the hydrogel system for 2D and 3D cultivation of various stromal cell lines such as fibroblasts, myoblasts and endothelial cells, in order to establish novel tissue engineering platform *in vitro*. Hydrogel-based cultivation of endothelial cells would be of particular interest since its proliferation and patterning heavily rely on the recruitment of multiple growth factors to the local microenvironment, a process in which sulfation could play a critical role.

Collectively, these results indicate that sulfation is a tunable design parameter that can be used to adjust pore architecture, mechanics, enzymatic stability and size- and charge-selective transport in these thermoresponsive hydrogels. While sulfation increases swelling and alters rheological behaviour, it also confers increased enzymatic stability, enables size-selective molecular diffusion, and exhibits cell type-specific effects on viability. The ability to maintain efficient transport of small molecules while selectively retarding protein diffusion may offer unique advantages for applications that require controlled microenvironments and regulated availability of signalling or growth-promoting factors. These findings identify sulfation as a tunable design parameter for thermoresponsive synthetic hydrogels and provide a mechanistic basis for tailoring such materials for advanced cell culture and, in future, application-specific biomedical use.

Author contributions

Lasse Riediger (investigation; methodology: lead; project administration: supporting; visualization: lead; writing – original draft: lead; writing – review & editing: supporting). Lei Wang (investigation: supporting; methodology: supporting). Peer Nölte (investigation: supporting; methodology: supporting). Cosmin Butnarasu (investigation: supporting; methodology: supporting). Peng Tang (investigation: supporting; methodology: supporting). Yannic Kerkhoff (investigation: supporting; methodology: supporting). Elisa Quaas (investigation: supporting; methodology: supporting). Justin Arenhoevel (investigation: supporting; methodology: supporting). Daniel Christian Lauster (project administration: supporting; supervision: supporting; writing – original draft: supporting). Yi-An Yang (conceptualization: equal; funding acquisition: equal; project administration: equal; supervision: equal; writing – original draft: lead; writing – review & editing: equal). Nan Ma (conceptualization: equal; funding acquisition: equal; project administration: equal; supervision: equal, writing – original draft: equal; writing – review & editing: equal). Rainer Haag (conceptualization: equal; funding acquisition: equal; project administration: equal; supervision: equal; writing – original draft: equal; writing – review & editing: equal).

Conflicts of interest

There are no conflicts to declare.

Data availability

The data that support the findings of this study are available in the supplementary information (SI). Supplementary information is available. See DOI: https://doi.org/10.1039/d5ma01183c.

Additional data can be accessed from the corresponding authors upon reasonable request.

Acknowledgements

Lasse Riediger and Yi-An Yang are funded by the Berliner Senatsverwaltung Berliner StartUp Stipendium HEALTH; Deutsche Forschungsgemeinschaft (DFG, German Research Foundation) – Project ID 431232613 – SFB 1449; and Investitionsbank Berlin Brandenburg, ProValid and greenCHEM as a transfer initiative sponsored by the Federal Ministry of Research, Technology and Space (BMFTR) ''T!Raum – TransferRäume für die Zukunft von Regionen'' of the Innovation und Strukturwandel'' – Project ID 2024000169. Lei Wang gratefully acknowledges the support of the China Scholarship Council (CSC) (Grant No. 202208440012). Furthermore, the authors acknowledge support from the SupraFAB research building realized with funds from the federal government and the city of Berlin and the Core Facility BioSupraMol supported by the DFG for their assistance and service.

Notes and references

1 Z. Chen, C. Du, S. Liu, J. Liu, Y. Yang, L. Dong, W. Zhao and W. Huang, *Giant*, 2024, **19**, 100323.

© 2026 The Author(s). Published by the Royal Society of Chemistry

Open Access Article. Published on 30 December 2025. Downloaded on 2/25/2026 1:52:12 AM. This article is licensed under a Creative Commons Attribution 3.0 Unported Licence.

2 P. Lu, D. Ruan, M. Huang, M. Tian, K. Zhu, Z. Gan and Z. Xiao, *Signal Transduction Targeted Ther.*, 2024, **9**, 166.
3 A. S. Hoffman, *Adv. Drug Delivery Rev.*, 2012, **64**, 18–23.
4 L. Klouda and A. G. Mikos, *Eur. J. Pharm. Biopharm.*, 2008, **68**, 34–45.
5 M. A. Ward and T. K. Georgiou, *Polymers*, 2011, **3**, 1215–1242.
6 A. Chakraborty, S. Alexander, W. Luo, N. Al-Salam, M. Van Oirschot, S. H. Ranganath, S. Chakrabarti and A. Paul, *Interdiscip. Med.*, 2023, **1**, e20230008.
7 E. A. Phelps, N. O. Enemchukwu, V. F. Fiore, J. C. Sy, N. Murthy, T. A. Sulchek, T. H. Barker and A. J. García, *Adv. Mater.*, 2012, **24**(64–70), 62.
8 J. Rosenquist, M. Folkesson, L. Höglund, J. Pupkaite, J. Hilborn and A. Samanta, *ACS Appl. Mater. Interfaces*, 2023, **15**, 34407–34418.
9 M. P. Lutolf and J. A. Hubbell, *Nat. Biotechnol.*, 2005, **23**, 47–55.
10 S. L. Scinto, D. A. Bilodeau, R. Hincapie, W. Lee, S. S. Nguyen, M. Xu, C. W. Am Ende, M. G. Finn, K. Lang, Q. Lin, J. P. Pezacki, J. A. Prescher, M. S. Robillard and J. M. Fox, *Nat. Rev. Methods Primers*, 2021, **1**, 30.
11 P. Dey, T. Schneider, L. Chiappisi, M. Gradzielski, G. Schulze-Tanzil and R. Haag, *Macromol. Biosci.*, 2016, **16**, 580–590.
12 Y. Long, M. Dimde, J. M. Adler, R. M. Vidal, T. L. Povolotsky, P. Nickl, K. Achazi, J. Trimpert, B. B. Kaufer, R. Haag and C. Nie, *ACS Appl. Mater. Interfaces*, 2024, **16**, 67504–67513.
13 I. Capila and R. J. Linhardt, *Angew. Chem., Int. Ed.*, 2002, **41**, 390–412.
14 J. Dernedde, A. Rausch, M. Weinhart, S. Enders, R. Tauber, K. Licha, M. Schirner, U. Zugel, A. von Bonin and R. Haag, *Proc. Natl. Acad. Sci. U. S. A.*, 2010, **107**, 19679–19684.
15 N. Rades, K. Licha and R. Haag, *Polymers*, 2018, **10** 595.
16 U. Freudenberg, P. Atallah, Y. D. P. Limasale and C. Werner, *Faraday Discuss.*, 2019, **219**, 244–251.
17 J. Turnbull, A. Powell and S. Guimond, *Trends Cell Biol.*, 2001, **11**, 75–82.
18 A. Zieris, R. Dockhorn, A. Rohrich, R. Zimmermann, M. Muller, P. B. Welzel, M. V. Tsurkan, J. U. Sommer, U. Freudenberg and C. Werner, *Biomacromolecules*, 2014, **15**, 4439–4446.
19 P. Atallah, L. Schirmer, M. Tsurkan, Y. D. Putra Limasale, R. Zimmermann, C. Werner and U. Freudenberg, *Biomaterials*, 2018, **181**, 227–239.
20 E. Öztürk, Ø. Arlov, S. Aksel, L. Li, D. M. Ornitz, G. Skjåk-Bræk and M. Zenobi-Wong, *Adv. Funct. Mater.*, 2016, **26**, 3649–3662.
21 K. Nagase, M. Yamato, H. Kanazawa and T. Okano, *Biomaterials*, 2018, **153**, 27–48.
22 H. G. Schild, *Prog. Polym. Sci.*, 1992, **17**, 163–249.
23 M. A. Cooperstein and H. E. Canavan, *Biointerphases*, 2013, **8**, 19.
24 S. Abbina, S. Vappala, P. Kumar, E. M. J. Siren, C. C. La, U. Abbasi, D. E. Brooks and J. N. Kizhakkedathu, *J. Mater. Chem. B*, 2017, **5**, 9249–9277.
25 M. Calderón, M. A. Quadir, S. K. Sharma and R. Haag, *Adv. Mater.*, 2010, **22**, 190–218.
26 M. Weinhart, T. Becherer, N. Schnurbusch, K. Schwibbert, H.-J. Kunte and R. Haag, *Adv. Eng. Mater.*, 2011, **13**, B501–B510.
27 S. J. Bryant and K. S. Anseth, *J. Biomed. Mater. Res.*, 2002, **59**, 63–72.
28 G. D. Nicodemus and S. J. Bryant, *Tissue Eng., Part B*, 2008, **14**, 149–165.
29 T. Stylianopoulos, B. Diop-Frimpong, L. L. Munn and R. K. Jain, *Biophys. J.*, 2010, **99**, 3119–3128.
30 E. S. Place, N. D. Evans and M. M. Stevens, *Nat. Mater.*, 2009, **8**, 457–470.
31 M. W. Tibbitt and K. S. Anseth, *Biotechnol. Bioeng.*, 2009, **103**, 655–663.
32 S. V. Murphy and A. Atala, *Nat. Biotechnol.*, 2014, **32**, 773–785.
33 G. Rossi, A. Manfrin and M. P. Lutolf, *Nat. Rev. Genet.*, 2018, **19**, 671–687.
34 G. Xu, K. Liu, B. Jia, Z. Dong, C. Zhang, X. Liu, Y. Qu, W. Li, M. Zhao, H. Zhou and Y.-Q. Li, *ACS Nano*, 2024, **18**, 3814–3825.
35 K. Braeckmans, L. Peeters, N. N. Sanders, S. C. De Smedt and J. Demeester, *Biophys. J.*, 2003, **85**, 2240–2252.
36 H. Deschout, F. Cella Zanacchi, M. Mlodzianoski, A. Diaspro, J. Bewersdorf, S. T. Hess and K. Braeckmans, *Nat. Methods*, 2014, **11**, 253–266.
37 M. Hellmund, K. Achazi, F. Neumann, B. N. Thota, N. Ma and R. Haag, *Biomater. Sci.*, 2015, **3**, 1459–1465.
38 J. Arenhoevel, A. Kuppe, A. Addante, L. F. Wei, N. Boback, C. Butnarasu, Y. Zhong, C. Wong, S. Y. Graeber, J. Duerr, M. Gradzielski, D. Lauster, M. A. Mall and R. Haag, *Biomater. Sci.*, 2024, **12**, 4376–4385.
39 Y. Kerkhoff, H. Rulff, P. Mönch, C. Gutwein, A. Loewe, S. Timm, R. Urbantat, K. Ludwig, R. Haag, M. Gradzielski, M. Mall, B. Siegmund and M. Ochs, Efficient AI-supported quantification of network structures in SEM imaged human mucus, ''ChemRxiv, 2025, preprint, DOI: 10.26434/chemrxiv-2025-qz5bj This content is a preprint and has not been peer-reviewed.'' ed., 2025.
40 L. Wang, L. Riediger, Q. Rao, X. Xu, Y. Nie, Y. Zhou, J. Zhang, P. Tang, W. Wang, F. Tacke, A. Guillot, L. Vallier, I. Talon, W. Li, Y.-A. Yang, R. Haag and N. Ma, *Adv. Funct. Mater.*, 2025, e08430.
41 T. S. Hebner, B. E. Kirkpatrick, B. D. Fairbanks, C. N. Bowman, K. S. Anseth and D. S. W. Benoit, *Adv. Sci.*, 2024, **11**, e2402191.
42 S. Thönes, S. Rother, T. Wippold, J. Blaszkiewicz, K. Balamurugan, S. Moeller, G. Ruiz-Gómez, M. Schnabelrauch, D. Scharnweber, A. Saalbach, J. Rademann, M. T. Pisabarro, V. Hintze and U. Anderegg, *Acta Biomater.*, 2019, **86**, 135–147.
43 L. Massi, A. Najer, R. Chapman, C. D. Spicer, V. Nele, J. Che, M. A. Booth, J. J. Doutch and M. M. Stevens, *J. Mater. Chem. B*, 2020, **8**, 8894–8907.
44 Q. Ran, X. Xu, P. Dey, S. Yu, Y. Lu, J. Dzubiella, R. Haag and M. Ballauff, *J. Chem. Phys.*, 2018, **149**, 163324.

Open Access Article. Published on 30 December 2025. Downloaded on 2/25/2026 1:52:12 AM.
This article is licensed under a Creative Commons Attribution 3.0 Unported Licence.

45 S. Yu, X. Xu, C. Yigit, M. van der Giet, W. Zidek, J. Jankowski, J. Dzubiella and M. Ballauff, *Soft Matter*, 2015, **11**, 4630–4639.
46 F. Reisbeck, A. Ozimkovski, M. Cherri, M. Dimde, E. Quaas, E. Mohammadifar, K. Achazi and R. Haag, *Polymers*, 2021, **13**(6), 982.
47 A. Sousa-Herves, P. Würfel, N. Wegner, J. Khandare, K. Licha, R. Haag, P. Welker and M. Calderón, *Nanoscale*, 2015, **7**, 3923–3932.
48 B. J. Zern, H. Chu and Y. Wang, *PLoS One*, 2010, **5**, e11017.
49 Ş. ComŞA, A. M. CÎMpean and M. Raica, *Anticancer Res.*, 2015, **35**, 3147.
50 Y. Jiang, Z. Ding, T. Ma, L. Zhou, Z. Ding, M. Adeli, X. Wang, L. Cheng, L. Ma, C. Cheng and H. Luo, *Adv. Funct. Mater.*, 2025, **35**, 2424512.
51 M. Delehedde, E. Deudon, B. Boilly and H. Hondermarck, *Bull. Cancer*, 1996, **83**, 129–134.
52 C. Koutsakis, A.-G. Tavianatou, D. Kokoretsis, G. Baroutas and N. K. Karamanos, *Biomolecules*, 2021, **11**, 1916.

© 2026 The Author(s). Published by the Royal Society of Chemistry